Non-Abelian wormholes threaded by a Yang-Mills-Higgs field in the BPS limit

Xiao Yan Chew[1,2,*] and Kok-Geng Lim[3,†]

[1]*Department of Physics Education, Pusan National University, Busan 46241, Republic of Korea*
[2]*Research Center for Dielectric and Advanced Matter Physics, Pusan National University, Busan 46241, Republic of Korea*
[3]*University of Southampton Malaysia, 79200 Iskandar Puteri, Johor, Malaysia*

(Received 7 October 2020; accepted 1 December 2020; published 29 December 2020)

In the Bogomol'nyi-Prasad-Sommerfield (BPS) limit of Einstein-Yang-Mills-Higgs theory, we construct numerically a non-Abelian wormhole supported by a phantom field. The probe limit is the Yang-Mills-Higgs field in the background of Ellis wormhole when the gravity is switched off. The wormhole solutions possess the Yang-Mills-Higgs hair in the presence of gravity; thus a branch of hairy wormhole solutions emerge from the Ellis wormhole when the gravitational coupling constant increases. We find that the masses of the wormholes and the scalar charge of the phantom field increase monotonically when the gravitational coupling constant increases. The wormhole spacetime possesses a double-throat configuration when the gravitational strength exceeds a critical value. Surprisingly, the wormholes satisfy the null energy condition at large gravitational strength. We also briefly discuss the redshift factor.

DOI: 10.1103/PhysRevD.102.124068

I. INTRODUCTION

It is well known that the SU(2) Yang-Mills-Higgs (YMH) theory with a Higgs field in the adjoint representation possesses both magnetic monopole [1,2] and multimonopole [3–6] solutions with finite energy. The 't Hooft–Polyakov magnetic monopole [1,2] is the first solitonic monopole solution in non-Abelian YMH theory with spontaneously broken symmetry. The exact solutions of the magnetic monopole and multimonopole are only found in the Bogomol'nyi-Prasad-Sommerfield (BPS) limit with vanishing Higgs self-interaction potential and satisfy the first-order Bogomol'nyi equation [7,8]. Their mass also saturates the lower bound, which is the Bogomol'nyi bound [8]. However, the numerical solutions can only be found beyond the BPS limit when the Higgs potential is nonvanishing [9]. There exist unstable and saddle-point solutions which do not satisfy the Bogomol'nyi equation, but they are only solutions to the second-order equations of motion of YMH theory—for instance, the monopole-antimonopole pair [10] and monopole-antimonopole chain solutions [11,12].

In the Einstein-Yang-Mills-Higgs (EYMH) system, where the YMH field is coupled with gravity, a branch of gravitating monopole solutions emerges from the 't Hooft–Polyakov monopole in flat space [13–21]. In the BPS limit, the mass of the gravitating monopole decreases monotonically as the gravitational strength increases. When the gravitational strength reaches a critical value, the solutions of the gravitating monopole end up as an extremal Reissner-Nordstrom black hole. This also occurs for static axially symmetric gravitating monopole solutions [22,23]. The counterpart EYMH black holes also exist, and they possess a non-Abelian gauge field outside the event horizon. Hence, they are also dubbed as the "black hole within monopole" [14,16], which is a counterexample to the "no hair" conjecture for black holes. The monopole-antimonopole pairs [23–29] and vortex rings [30,31] can also be constructed in the EYMH system.

Recently, a type of non-Abelian wormhole has been obtained numerically in the Einstein-Yang-Mills (EYM) system where the throat of the wormhole is supported by a phantom field [32]. These hairy wormholes solutions possess a sequence of solutions, which are labeled by the node number k of the gauge field function. They are analogous to the Bartnik-McKinnon solutions, which are the regular and spherically symmetric solutions of the EYM system [33]. A phantom field is a real-valued scalar field which has an opposite sign for the kinetic term. It can be used to model the accelerated expansion of our Universe in cosmology [34–37] and to construct some compact objects such as black holes [38,39], black rings [40], star-like objects [41], and wormholes [42–44].

The construction of traversable wormholes in GR usually requires the violation of the energy condition [45] to

*xychew998@gmail.com, xiao.yan.chew@uni-oldenburg.de
†K.G.Lim@soton.ac.uk

prevent the collapse of the throat.[1] A classic example of such a traversable wormhole is the static Ellis wormhole, which is supported by the phantom field [42–44]. However, the Ellis wormhole possesses unstable radial modes [49–51]. The static Ellis wormhole has also been generalized to the higher-dimensional case [51], to the slowly rotating case with perturbative methods [52,53], to the rapidly rotating case in four [54,55] and five dimensions with equal angular momenta [56], and also to the modified gravity—e.g., the scalar-tensor theory [57].

Furthermore, several astrophysical signatures of wormholes have been proposed in order to search for their existence in the near future, since they might mimic black holes: for example, the shadow [58–60], the gravitational lensing [61–67], the accretion disk around the wormhole [68], and the ringdown phase in the emission of gravitational waves [69].

Although there are also some wormhole-like structures in EYMH theory reported in Refs. [70–72], the wormholes in EYMH theory with a phantom field have not been explored yet. In this paper, our motivation is based on the solutions of particle-like and black holes in EYMH theory giving rise to new and interesting phenomena due to the presence of a non-Abelian field. Since the counterpart EYMH black hole exists, the wormhole configuration with non-Abelian YMH hair should also exist. Thus, we follow the approach of Ref. [32] to numerically obtain the symmetric wormhole solutions in EYMH with a phantom field in the BPS limit and study their properties in this paper. Our paper is organized as follows: In Sec. II, we briefly introduce the YMH theory and present the equations of motion. Subsequently, we derive the ordinary differential equations (ODEs) from the equations of motion. We then introduce the geometrical properties, the global charges, the null energy condition of wormholes, and the boundary conditions imposed on the ODEs. In Sec. III, we exhibit and discuss our numerical results. In Sec. IV, we conclude our research works and briefly discuss the stability of the solutions and the possible outlook from this present work.

II. THEORETICAL FRAMEWORK

A. Theory and *Ansätze*

In the Einstein-Hilbert action, we consider Einstein gravity to be coupled with a phantom field ψ and a gauge field A_μ in SU(2) YMH theory in the BPS limit:

$$S_{\rm EH} = \int d^4x\sqrt{-g}\left[\frac{R}{16\pi G} + \mathcal{L}_{\rm ph} + \mathcal{L}_{\rm YMH}\right], \tag{1}$$

where the Lagrangian of the phantom field and YMH [23] are given, respectively, by

$$\mathcal{L}_{\rm ph} = \frac{1}{2}\partial_\mu\psi\partial^\mu\psi,$$
$$\mathcal{L}_{\rm YMH} = -\frac{1}{2}{\rm Tr}(F_{\mu\nu}F^{\mu\nu}) - \frac{1}{4}{\rm Tr}(D_\mu\Phi D^\mu\Phi). \tag{2}$$

The covariant derivative of the Higgs field and the gauge field strength tensor are given, respectively, by

$$F_{\mu\nu} = \partial_\mu A_\nu - \partial_\nu A_\mu + ie[A_\mu, A_\nu], \tag{3}$$

$$D_\mu\Phi = \partial_\mu\Phi + ie[A_\mu, \Phi], \tag{4}$$

where $A_\mu = \frac{1}{2}\tau^a A^a_\mu$ and $\Phi = \phi^a\tau^a$, with τ^a being the Pauli matrices.

By varying the action with respect to the metric $g_{\mu\nu}$, we obtain the Einstein equation,

$$R_{\mu\nu} - \frac{1}{2}g_{\mu\nu}R = \beta(T^{\rm ph}_{\mu\nu} + T^{\rm YMH}_{\mu\nu}), \tag{5}$$

where $\beta = 8\pi G$, and the stress-energy tensors for the phantom field $T^{\rm ph}_{\mu\nu}$ and YMH $T^{\rm YMH}_{\mu\nu}$ are given, respectively, by

$$T^{\rm ph}_{\mu\nu} = \frac{1}{2}g_{\mu\nu}\partial_\alpha\psi\partial^\alpha\psi - \partial_\mu\psi\partial_\nu\psi, \tag{6}$$

$$T^{\rm YMH}_{\mu\nu} = {\rm Tr}\left(\frac{1}{2}D_\mu\Phi D_\nu\Phi - \frac{1}{4}g_{\mu\mu}D_\alpha\Phi D^\nu\Phi\right) + 2{\rm Tr}\left(g^{\alpha\beta}F_{\mu\alpha}F_{\nu\beta} - \frac{1}{4}g_{\mu\nu}F_{\alpha\beta}F^{\alpha\beta}\right). \tag{7}$$

The equations of motion for the matter fields are

$$\frac{1}{\sqrt{-g}}\partial_\mu(\sqrt{-g}\partial^\mu\psi) = 0, \qquad D_\mu F^{\mu\nu} = \frac{ie}{4}[\Phi, D^\nu\Phi],$$
$$D_\mu D^\mu\Phi = 0. \tag{8}$$

We employ the following line element to construct a globally regular wormhole spacetime:

$$ds^2 = -F_0(\eta)dt^2 + F_1(\eta)[d\eta^2 + h(\eta)(d\theta^2 + \sin^2\theta d\varphi^2)], \tag{9}$$

where $h(\eta) = \eta^2 + \eta_0^2$, with η_0 as the throat parameter. The wormhole spacetime possesses two asymptotically flat regions in the limit $\eta \to \pm\infty$.

Likewise, we employ the spherically symmetric *Ansatz* in a purely magnetic gauge field ($A_t = 0$) for the gauge and Higgs field [16]:

$$A_\mu dx^\mu = \frac{1 - K(\eta)}{2e}(\tau_\varphi d\theta - \tau_\theta\sin\theta d\varphi), \qquad \Phi = H(\eta)\tau_\eta. \tag{10}$$

[1]However, there are wormhole solutions that can be constructed in the modified theory of gravity without exotic matter [46–48].

B. Ordinary differential equations (ODEs)

We set the constant $e = 1$. By substituting Eqs. (9) and (10) into the Einstein equation Eq. (5) and equations of motion for the gauge fields [Eq. (8)], we obtain a set of second-order and nonlinear ODEs for the metric functions:

$$F_1'' + \frac{2\eta}{h}F_1' - \frac{3F_1'^2}{4F_1} + \frac{\eta_0^2 F_1}{h^2} = \beta\frac{F_1}{2}\psi'^2 - \beta\frac{(K^2-1)^2 + 2hK'^2 + h^2F_1H'^2 + 2hF_1H^2K^2}{2h^2}, \tag{11}$$

$$\left(\frac{F_1'}{2F_1} + \frac{\eta}{h}\right)\frac{F_0'}{F_0} + \frac{F_1'^2}{4F_1^2} + \frac{\eta}{hF_1}F_1' - \frac{\eta_0^2}{h^2} = -\frac{\beta}{2}\psi'^2 + \beta\frac{-(K^2-1)^2 + 2hK'^2 + h^2F_1H'^2 - 2hF_1H^2K^2}{2h^2F_1}, \tag{12}$$

$$F_0'' + \left(-\frac{F_0'}{2F_0} + \frac{\eta}{h}\right)F_0' + \frac{F_0}{F_1}F_1'' + \left(-\frac{F_1'}{F_1} + \frac{\eta}{h}\right)\frac{F_0F_1'}{F_1} + \frac{2F_0\eta_0^2}{h^2} = \beta F_0\psi'^2 - F_0\left[\frac{-(K^2-1)^2 + h^2F_1H'^2}{h^2F_1}\right]. \tag{13}$$

$$K'' + \frac{1}{2}\left(\frac{F_0'}{F_0} - \frac{F_1'}{F_1}\right)K' - \frac{K(K^2 - 1 + hF_1H^2)}{h} = 0, \tag{14}$$

$$H'' + \frac{1}{2}\left(\frac{F_0'}{F_0} + \frac{F_1'}{F_1} + \frac{4\eta}{h}\right)H' - \frac{2K^2}{h} = 0, \tag{15}$$

where the prime denotes a derivative of the functions with respect to the radial coordinate η.

We obtain a first-order integral from Eq. (8) for the phantom field:

$$\psi' = \frac{D}{h\sqrt{F_0F_1}}, \tag{16}$$

where D is the scalar charge of the phantom field. Then we replace the term ψ'^2 by substituting $\psi' = D/(h\sqrt{F_0F_1})$ into Eqs. (11)–(13).

We solve Eqs. (11), (13), (14), and (15) numerically with Eq. (12), which is expressed as

$$D^2 = \frac{2h^2F_0F_1}{\beta}\left[-\left(\frac{F_1'}{2F_1} + \frac{\eta}{h}\right)\frac{F_0'}{F_0} - \frac{F_1'^2}{4F_1^2} - \frac{\eta}{hF_1}F_1' + \frac{\eta_0^2}{h^2} + \beta\frac{-(K^2-1)^2 + 2hK'^2 + h^2F_1H'^2 - 2hF_1H^2K^2}{2h^2F_1}\right] \tag{17}$$

to monitor the quality of the numerical solutions with the condition $D^2 = \text{const}$.

C. Geometrical properties

We introduce $R(\eta)^2$ as the shape function for studying the geometry of a wormhole:

$$R(\eta)^2 = F_1h. \tag{18}$$

Note that $R(\eta)$ is the circumferential radius of the wormhole and should not contain zero for a globally regular wormhole solution. When R contains a local minimum, which is known as a throat of the wormhole, then the wormhole possesses a minimal surface area at the throat. However, if R contains a local maximum, then it is an equator of the wormhole, which corresponds to the maximal surface area of the wormhole.

For simplicity, we consider the metric functions symmetric with respect to the coordinate $\eta = 0$, so we assume that the circumferential radius of the wormhole at $\eta = 0$ could be either a throat or an equator, which implies that R should have an extremum at $\eta = 0$ by requiring

$$R'(0) = 0 \Rightarrow \left.\frac{(hF_1' + 2\eta F_1)}{2R}\right|_{\eta=0} = 0, \tag{19}$$

where we have to set $F_1'(0) = 0$. In particular, if the wormhole only contains a single throat, then the throat must be located at $\eta = 0$ with the minimal surface area $A_{\text{th}} = 4\pi R(0)^2 = 4\pi F_1(0)\eta_0^2$.

Furthermore, the second-order derivative of R at $\eta = 0$ is given by

$$R''(0) = \left.\frac{2F_1 + hF_1''}{2R}\right|_{\eta=0} = \frac{F_1}{R}, \tag{20}$$

where we have used $F_1''(0)$ from the ODEs. The wormhole possesses either a throat or an equator at $\eta = 0$, which can be determined from the conditions $R''(0) > 0$ or $R''(0) < 0$, respectively. Since $R''(0) > 0$, $R(0)$ always remains a throat.

Note that when $R'(\eta_{\rm crit}) = R''(\eta_{\rm crit}) = 0$, the circumferential radius forms a turning point at some value of the radial coordinate $\eta_{\rm crit}$, and the geometry of the wormhole is in a transition state in which the double throat and the equator can simultaneously exist; this also implies that a transition can occur from the single-throat configuration to the double-throat configuration [73,74].

In addition, we can visualize the wormhole throat in the equatorial plane ($\theta = \pi/2$) by embedding the equatorial plane using the cylindrical coordinates (ρ, φ, z) in Euclidean space:

$$ds^2 = F_1 d\eta^2 + hF_1 d\varphi^2, \tag{21}$$

$$= d\rho^2 + dz^2 + \rho^2 d\varphi^2. \tag{22}$$

Hence, we obtain the expression for z from the comparison:

$$z = \pm \int \sqrt{F_1 - \left(\frac{d\rho}{d\eta}\right)^2}\, d\eta, \qquad \rho \equiv R. \tag{23}$$

We can also evaluate the surface gravity κ at the throat, which is defined as

$$\kappa^2 = -\frac{1}{2}(\nabla_\mu \zeta_\nu)(\nabla^\mu \zeta^\nu), \tag{24}$$

$$\Rightarrow \kappa = \frac{F_0'}{2\sqrt{F_0 F_1}}, \tag{25}$$

where $\zeta^\mu = (1, 0, 0, 0)$ is the timelike Killing vector. Equation (25) shows that κ vanishes for symmetric wormholes with a single throat but remains finite for wormholes with a double-throat configuration.

D. Global charges

The wormhole solutions possess mass M as the global charge associated with the asymptotic Killing vector ∂_t. The mass of the wormhole can be read off directly from the asymptotic expansion of the metric at $\eta \to \infty$,

$$F_0 \to 1 - \frac{2GM}{\eta}. \tag{26}$$

Recall that the charge of the phantom field is given by D^2. Then, the magnetic charge for the non-Abelian gauge fields is given by [75,76]

$$\mathcal{P}^{\rm YMH} = \frac{1}{4\pi} \oint \sqrt{\sum_i (F^i_{\theta\varphi})^2}\, d\theta d\varphi = |P|, \tag{27}$$

where the integral is evaluated at the spatial infinity, yielding $P = 0$ for the hairy wormholes [32].

E. Null energy condition (NEC)

Since the construction of a wormhole requires the violation of energy conditions, we can examine the NEC of the wormhole, which states that

$$T_{\mu\nu} k^\mu k^\nu \geq 0 \tag{28}$$

for all (future-pointing) null vectors k_μ. Note that the violation of the NEC also implies the violation of the weak and strong energy conditions.

Since the wormhole spacetime is spherically symmetric, there are two choices of null vector [48]:

$$k_\mu = \left(g_{tt}, \sqrt{-\frac{g_{tt}}{g_{\eta\eta}}}, 0, 0\right) \quad \text{and} \quad k_\mu = \left(1, 0, \sqrt{-\frac{g_{tt}}{g_{\theta\theta}}}, 0\right), \tag{29}$$

which yield two expressions to measure the violation of the NEC:

$$-T^t{}_t + T^\eta{}_\eta = -\frac{\psi'^2}{F_1} + \frac{H'^2}{F_1} + \frac{2K'^2}{hF_1^2} = -\frac{D^2}{h^2 F_0 F_1^2} + \frac{H'^2}{F_1} + \frac{2K'^2}{hF_1^2}, \tag{30}$$

$$-T^t{}_t + T^\theta{}_\theta = \frac{K'^2}{hF_1^2} + \frac{H^2 K^2}{hF_1} + \frac{(K^2-1)^2}{h^2 F_1^2} \geq 0. \tag{31}$$

F. Boundary conditions

Since we only consider the wormhole solutions with metric functions symmetric with respect to $\eta = 0$, we only integrate the ODEs from $\eta = 0$ to infinity. We impose eight boundary conditions at $\eta = 0$ and $\eta = \infty$. First, we require that the first-order derivative of the metric functions vanish at the throat:

$$F_0'(0) = F_1'(0) = 0. \tag{32}$$

These conditions imply that the metric functions possess the extremum at $\eta = 0$. At infinity, the metric functions approach Minkowski spacetime:

$$F_0(\infty) = F_1(\infty) = 1. \tag{33}$$

We impose the following boundary conditions for the gauge fields by fixing their values at $\eta = 0$, and they satisfy the asymptotic flatness at infinity:

$$K(0) = 1, \qquad H(0) = 0, \qquad K(\infty) = 0, \qquad H(\infty) = 1. \tag{34}$$

We solve the set of ODEs numerically using Colsys, which solves boundary value problems for systems of

nonlinear coupled ODEs based on the Newton-Raphson method [77]. We scale the parameters by the throat parameter η_0:

$$\eta \to \eta_0 \eta, \qquad h \to \eta_0^2 h, \qquad \beta \to \eta_0^2 \beta, \qquad H \to \frac{H}{\eta_0}. \tag{35}$$

Thus, we introduce a mass parameter μ, which is given by

$$\mu = \frac{\beta M}{8\pi\eta_0}. \tag{36}$$

We compactify the radial coordinate η by $\eta = \eta_0 \tan(\pi x/2)$ in the numerics.

III. RESULTS AND DISCUSSIONS

A. Probe limit

We start our investigation from the probe limit of the wormhole in the BPS limit. When the gravity is switched off ($\beta = 0$), we see that the YMH field does not contribute to the Einstein equation from Eqs. (11)–(13). Therefore, the metric in Eq. (9) is the massless Ellis wormhole $[F_0(\eta) = F_1(\eta) = 1]$, which is symmetric. The phantom field is given by

$$\psi = \frac{D}{\eta_0}\left[\arctan\left(\frac{\eta}{\eta_0}\right) - \frac{\pi}{2}\right]. \tag{37}$$

The pure YMH equations in the background of the Ellis wormhole are then simplifed to

$$K'' = \frac{K(K^2 - 1 + hH^2)}{h}, \tag{38}$$

$$H'' = -\frac{2\eta}{h}H' + \frac{2K^2}{h}H. \tag{39}$$

The above ODEs are solved numerically and are shown in Fig. 1. Note that the 't Hooft–Polyakov monopole gives the solution of the YMH theory. The corresponding theory possesses an exact solution in the BPS limit [7], which is given by

$$K(R) = \frac{R}{\sinh(R)}, \qquad H(R) = \coth(R) - \frac{1}{R}. \tag{40}$$

The exact solution is stable, and its mass is unity.

B. With backreaction

We exhibit our numerical results by varying the gravitational coupling constant β in the range [0, 400]. The wormholes could take any real positive values of β; this is in contrast to a YM wormhole, where the limiting configuration is the extremal Reissner-Nordstrom black hole for higher nodes [32]. Recall that an Ellis wormhole is massless; its circumferential radius and scalar charge are unity. Since the gauge fields do not present, then the Ellis wormhole has the analogue of the Schwarzschild solution for the black holes [32]. When we increase β from zero, the solutions of hairy wormholes emerge from the Ellis wormhole; thus, the properties of these hairy wormholes differ from Ellis wormholes when β increases. Figure 2(a) shows that the hairy wormholes gain the mass when β increases from zero; the mass increases monotonically as β increases. Figure 2(b) shows that the scaled scalar charge of the phantom field increases monotonically from unity as β increases.

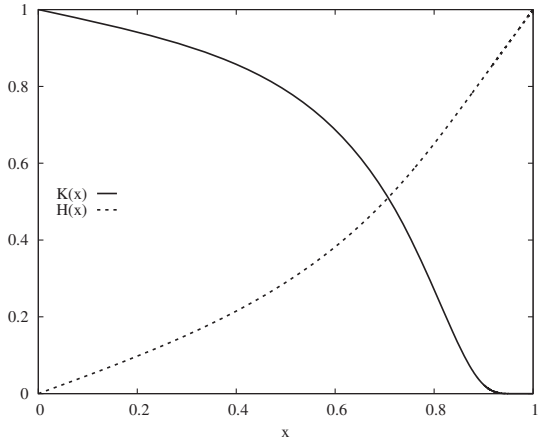

FIG. 1. The gauge fields $K(x)$ and $H(x)$ in the compactified coordinate x in the probe limit.

The metric component g_{tt} is relevant with the observer in the asymptotic region measuring the redshift factor z, which describes the effect of gravitational redshift on a photon being emitted from a source in the wormhole spacetime [78]:

$$z = \frac{\lambda_{\text{asym}}}{\lambda_{\text{emit}}} = \frac{\sqrt{-g_{tt}(\infty)}}{\sqrt{-g_{tt}(0)}} - 1 = \frac{1}{\sqrt{F_0(0)}} - 1, \tag{41}$$

where λ_{asym} is the wavelength measured by the observer and λ_{emit} is the wavelength of the photon in the wormhole. For simplicity, we consider the photon to be emitted at the throat $\eta = 0$. Figure 2(c) exhibits that the profile for the metric function F_0 is strictly increasing from $F_0(0)$ to the asymptotic value, but the value of $F_0(0)$ is strictly decreasing when β increases. This gives rise to the observer always measuring the wavelength of the photon as redshifted, as shown in Fig. 2(d). Similarly, the profile of the function F_1 in Fig. 2(e) is strictly decreasing from its maximum value at $\eta = 0$ to the asymptotic value. However, we find surprisingly that the wormholes still can possess a double-throat configuration, which we will discuss in detail in the next paragraph. In Fig. 2(f), the gauge field K decays faster, while the profile of gauge field H does not vary too much when β increases.

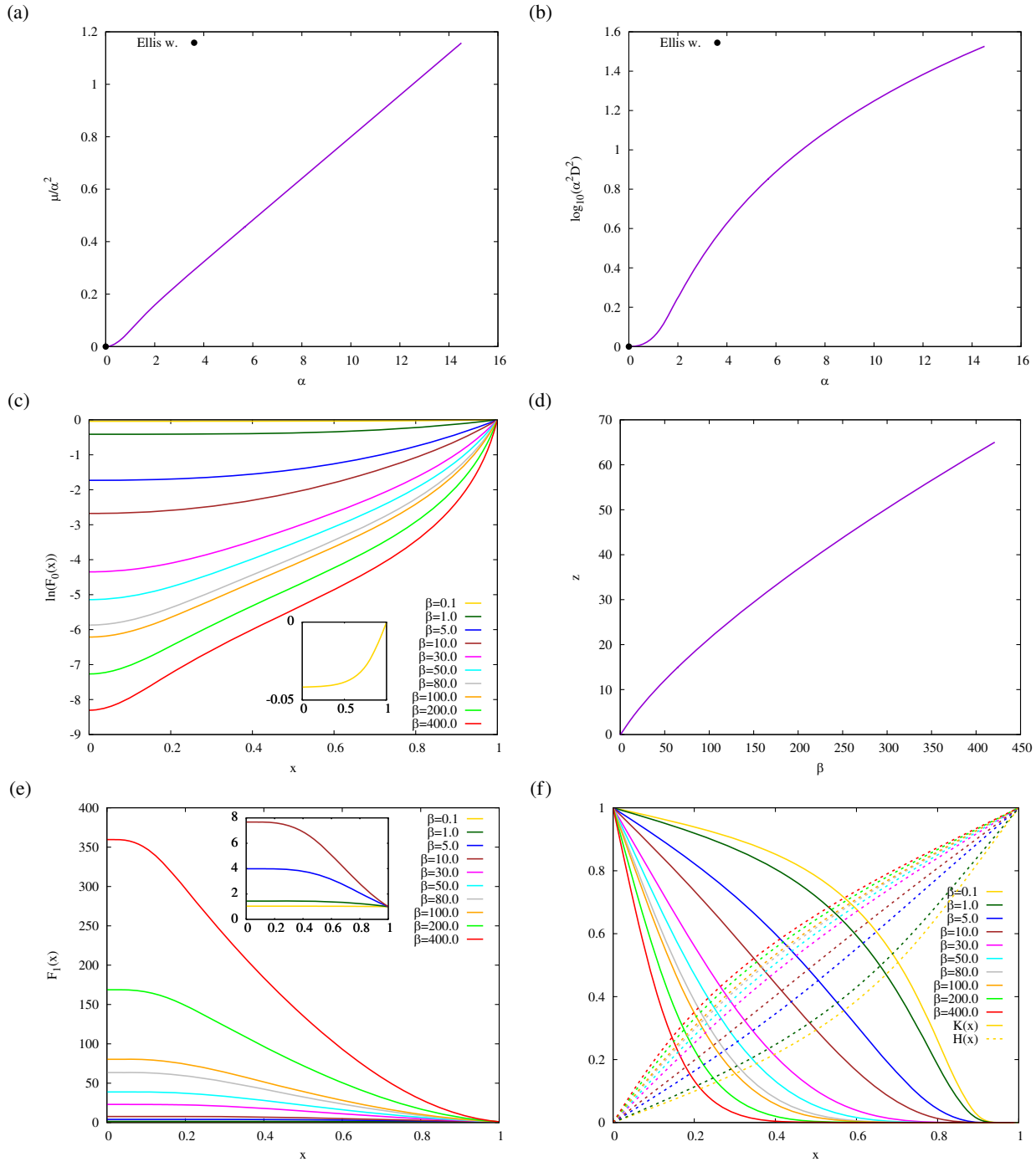

FIG. 2. (a) The scaled mass μ/α^2 versus the scaled gravitational coupling constant α. (b) The logarithmic scaled scalar charge $\log_{10}(\alpha^2 D^2)$ versus the scaled gravitational coupling constant α. (c) The metric function $\ln(F_0(x))$ in the compactified coordinate x for several values of β. (d) The gravitational redshift z versus the gravitational coupling strength β. (e) The metric function $F_1(x)$ in the compactified coordinate x for several values of β. (f) The gauge fields $K(x)$ and $H(x)$ for several values of β in the compactified coordinate x. The dot denotes the value for a massless Ellis wormhole.

Let us turn our discussion to the geometry of these hairy wormholes. Figure 3(a) shows that they possess only a single throat at $x = 0$ within the range $0 \leq \beta < \beta_{\text{crit}}$, since $R''(0) > 0$ in Fig. 3(b). Here β_{crit} is the critical value of β, which is approximately equal to 64.630655. When $\beta = \beta_{\text{crit}}$, we see that $R'(x_{\text{crit}}) = R''(x_{\text{crit}}) = 0$ in Fig. 3(b); at this stage the wormhole simultaneously develops a throat at x_{th} and an equator x_{eq} at $x \approx 0.32237$, while $x = 0$ is still maintained as a throat. This means that the transition from the single-throat configuration to the double-throat

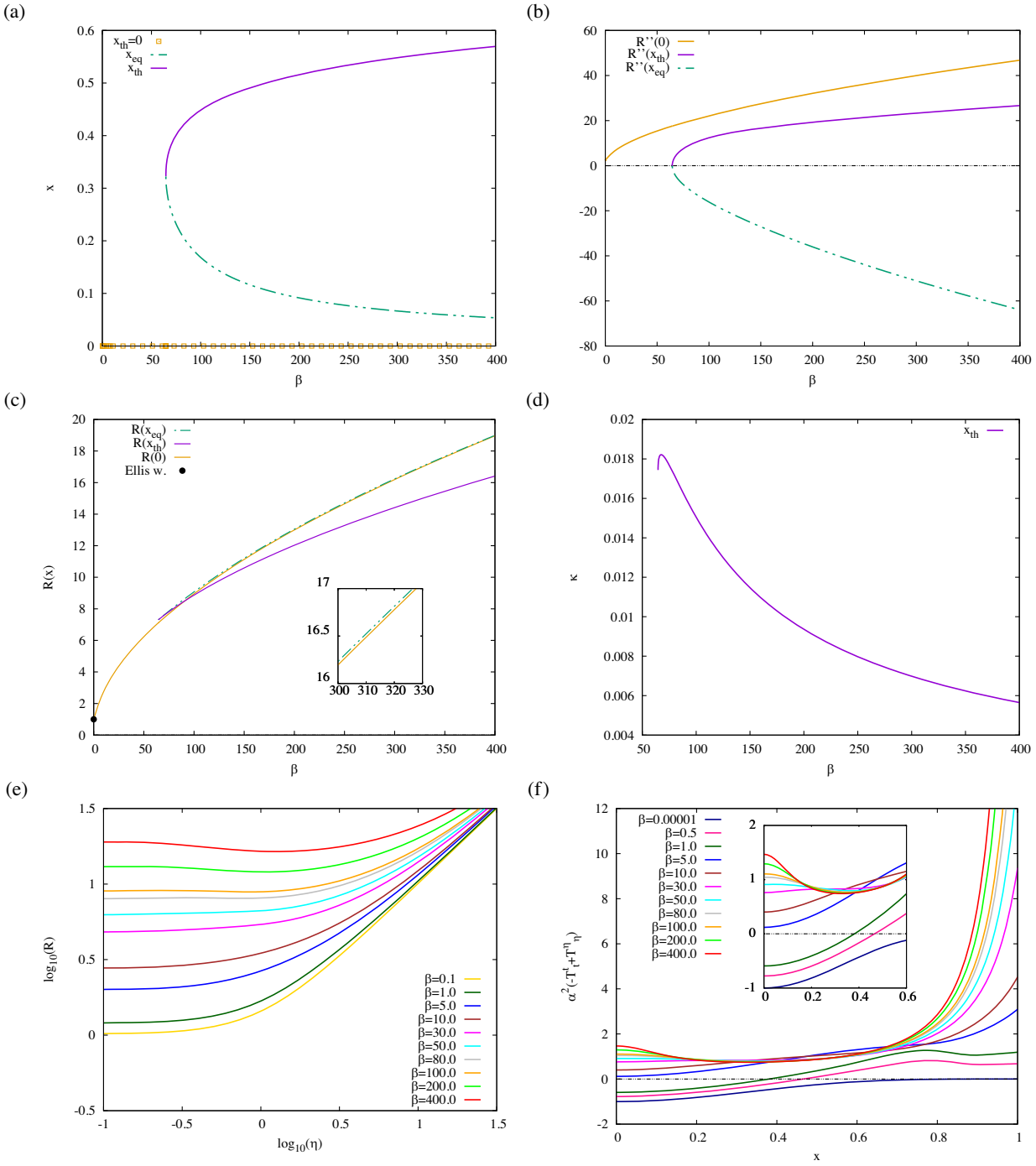

FIG. 3. The properties of wormhole solutions. (a) The location of throats and the equator versus the gravitational coupling constant β. (b) The second-order derivative of R in the compactified coordinate x for the throats and the equator versus the gravitational coupling constant β. (c) The circumferential radius of the throats $R(x_{\rm th})$ and the equator $R(x_{\rm eq})$ in the compactified coordinate x versus the gravitational coupling constant β. (d) The surface gravity κ at the throat $x_{\rm th}$ versus the gravitational coupling constant β. (e) The circumferential radius R of wormhole solutions for several values of β. (f) The violation of the scaled null energy condition (NEC) for the wormhole solutions with several values of β in the compactified coordinate x. The constant α is defined as $\beta = 2\alpha^2$. In (a)–(c), the yellow curve denotes the throat at $x = 0$. The green curve with a two-dashed line and the purple curve denote the equator $x_{\rm eq}$ and another throat at $x_{\rm th}$ in the compactified coordinate x, respectively.

configuration can happen when $\beta \geq \beta_{\rm crit}$, as shown in Fig. 3. In Fig. 3(a), the equator is always sandwiched between the throats $0 < x_{\rm eq} < x_{\rm th}$. We also observe that the location of the equator $x_{\rm eq}$ moves toward $x = 0$, and the location of another throat $x_{\rm th}$ moves away from $x = 0$; hence the equator and the throat at $x = 0$ are very close.

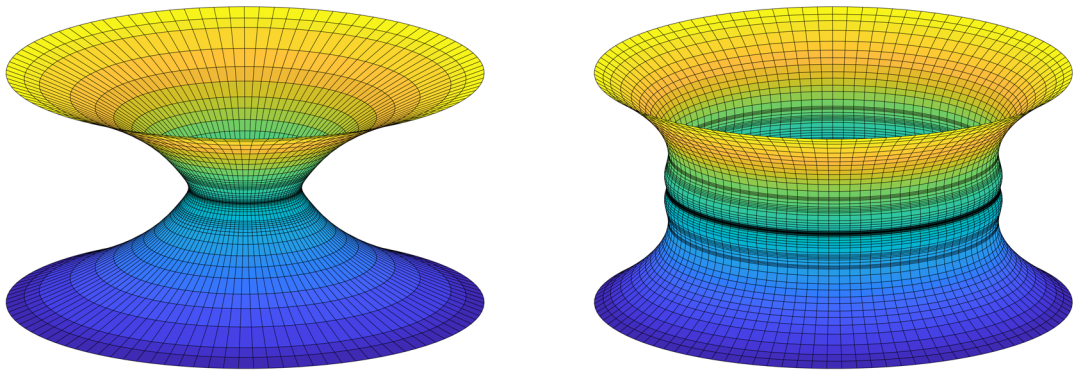

(a) (b)

FIG. 4. The isometric embedding of the wormholes in the Euclidean space for (a) $\beta = 10$ (single throat) and (b) $\beta = 100$ (double throat).

This gives rise to the circumferential radius of the equator being slightly larger than the circumferential radius of the throat at $x = 0$ for very large values of β, as shown in Fig. 3(c). Here $R(0)$ increases monotonically as β increases, which can be seen from Figs. 3(c) and 3(e).

When $\beta < \beta_{\text{crit}}$, the surface gravity κ vanishes for the wormholes with a single throat, since $F_0'(0) = 0$. However, another throat η_{th} appears in between the equator and the asymptotically flat region when $\beta = \beta_{\text{crit}}$; thus κ assumes a finite value, as shown in Fig. 3(d). When $\beta > \beta_{\text{crit}}$, κ increases to a maximum value and then decreases for very large values of β. Furthermore, we can visualize the single-throat and double-throat structures in the embedding diagrams, which are shown in Fig. 4.

In Fig. 3(f), we scale the NEC by $\alpha^2(-T_t^t + T_\eta^\eta)$, so that we can compare the NEC of our wormholes with the Ellis wormhole. We find that the violation of the NEC is the largest for the Ellis wormhole, particularly at the throat. When β increases, the violation of the NEC at the throat decreases, and the surprise is that the wormholes satisfy the NEC for large values of β. Note that the NEC vanishes at the asymptotic flat region for a very small value of β. However, the NEC assumes a finite value at the asymptotic flat region when β becomes very large—the reason is that the first and third terms vanish, but H' does not vanish [as can be seen from Fig. 2(f)]; thus the second term remains finite. In addition, the NEC at the infinity has been amplified due to the scaling factor α^2.

IV. CONCLUSION AND OUTLOOK

We have obtained the symmetric wormholes which are supported by the phantom field in the Einstein-Yang-Mills-Higgs (EYMH) system in the Bogomol'nyi-Prasad-Sommerfield (BPS) limit. When we switch off the gravity, we obtain the probe limit, which is the Yang-Mills-Higgs (YMH) field in the background of the Ellis wormhole. In the presence of gravity, the wormholes possess the nontrivial non-Abelian hair; thus, the hairy wormhole solutions emerge from the Ellis wormhole, where the wormholes gain the mass. The masses of wormholes and the scaled scalar charge of the phantom field increase monotonically when the gravitational coupling constant increases.

When the gravitational strength is below a critical value, the wormholes only possess a single throat at the radial coordinate $\eta = 0$; thus, the corresponding surface gravity vanishes. When the gravitational strength is equal to the critical value, an equator and another throat coexist simultaneously somewhere in the manifold; thus, the transition from the single-throat to the double-throat configuration can occur. The equator is sandwiched between the throat at $\eta = 0$ and another throat. Therefore, the surface gravity of another throat assumes finite values. The circumferential radius of the throat at $\eta = 0$ increases monotonically and still remains as the throat even in the strong gravitational field. The circumferential radius of the equator is slightly larger than the circumferential radius of the throat at $\eta = 0$ because they are very close to each other in the large gravitational coupling. The violation of the null energy condition is the largest for the Ellis wormhole, particularly at the throat. However, the violation of the null energy condition decreases when the gravitational strength increases. Thus, the wormholes satisfy the null energy condition in the strong gravitational strength.

Since we only study the properties of hairy wormholes with the vanishing Higgs self-interaction, a natural extension of this work would be to construct and investigate the properties of hairy wormholes with finite Higgs self-interaction. We have some preliminary results which show that the properties of hairy wormholes are different than the BPS case. With finite Higgs self-interaction, the masses of wormholes increase from zero but decrease very sharply when the gravitational strength reaches a critical value. The scaled scalar charge also increases very sharply

at the critical value of gravitational strength. The results (in preparation) will be reported elsewhere [79].

Concerning the stability issue of the wormholes, the wormhole solutions which are constructed by the phantom field are generically unstable against the linear perturbation [49–51,80–82]. Furthermore, the stability analysis has shown that the particle-like and hairy black hole solutions of the EYMH system are unstable [83–85]. Hence, we conjecture that the EYMH hairy wormholes are unstable as well, because they will inherit the instabilities from the Ellis wormholes and behave qualitatively unstable as the compact objects in the EYMH system. It would be of interest to carry out a full linear stability analysis of hairy wormholes consistently by perturbing all the functions. However, the presence of the YMH field could introduce an extra degree of freedom and cause the calculation of unstable modes to become nontrivial. Since the calculation of linear stability is tedious and requires a lot of effort, we leave this as an independent investigation. Nevertheless, the unstable modes disappear for sufficiently rapidly rotating Ellis wormholes in five dimensions with equal angular momenta [56]. Since the counterpart EYMH black holes can rotate, it is interesting to construct the rotating EYMH wormholes, which might be stable against the perturbations.

Since the static and regular EYMH solutions can also possess only axial symmetry and need not be spherically symmetric, their counterpart static black holes also can possess only an axially symmetric horizon [22,23], which is a counterexample to Israel's theorem. Therefore, as a first step to constructing the rotating wormholes in EYMH, we could consider constructing the static hairy wormhole solutions with a throat which is also axially symmetric.

ACKNOWLEDGMENTS

X. Y. C. acknowledges the useful discussion with Jose Luis Blázquez-Salcedo, Jutta Kunz, Yen Chin Ong, and Eugen Radu. X. Y. C. thanks the National Research Foundation of Korea (Grant No. 2018R1D1A1B07049126) for funding.

[1] G. 't Hooft, Nucl. Phys. **B79**, 276 (1974).
[2] A. M. Polyakov, JETP Lett. **20**, 194 (1974), http://www.jetpletters.ac.ru/ps/1789/article_27297.shtml.
[3] C. Rebbi and P. Rossi, Phys. Rev. D **22**, 2010 (1980).
[4] R. Ward, Commun. Math. Phys. **79**, 317 (1981).
[5] P. Forgács, Z. Horváth, and L. Palla, Phys. Lett. **99B**, 232 (1981).
[6] M. Prasad and P. Rossi, Phys. Rev. D **24**, 2182 (1981).
[7] M. Prasad and C. M. Sommerfield, Phys. Rev. Lett. **35**, 760 (1975).
[8] E. Bogomol'Nyi, Sov. J. Nucl. Phys. **24**, 449 (1976).
[9] B. Kleihaus, J. Kunz, and D. Tchrakian, Mod. Phys. Lett. A **13**, 2523 (1998).
[10] B. Kleihaus and J. Kunz, Phys. Rev. D **61**, 025003 (1999).
[11] B. Kleihaus, J. Kunz, and Y. Shnir, Phys. Lett. B **570**, 237 (2003).
[12] B. Kleihaus, J. Kunz, and Y. Shnir, Phys. Rev. D **70**, 065010 (2004).
[13] P. Breitenlohner, P. Forgacs, and D. Maison, Nucl. Phys. **B383**, 357 (1992).
[14] K. Lee, V. Nair, and E. J. Weinberg, Phys. Rev. D **45**, 2751 (1992).
[15] P. Breitenlohner, P. Forgacs, and D. Maison, Nucl. Phys. **B442**, 126 (1995).
[16] Y. Brihaye, B. Hartmann, and J. Kunz, Phys. Lett. B **441**, 77 (1998).
[17] A. Lue and E. J. Weinberg, Phys. Rev. D **60**, 084025 (1999).
[18] Y. Brihaye, B. Hartmann, J. Kunz, and N. Tell, Phys. Rev. D **60**, 104016 (1999).
[19] Y. Brihaye, B. Hartmann, and J. Kunz, Phys. Rev. D **62**, 044008 (2000).
[20] Y. Brihaye, F. Grard, and S. Hoorelbeke, Phys. Rev. D **62**, 044013 (2000).
[21] Y. Brihaye and B. Hartmann, Phys. Rev. D **66**, 064018 (2002).
[22] B. Hartmann, B. Kleihaus, and J. Kunz, Phys. Rev. Lett. **86**, 1422 (2001).
[23] B. Hartmann, B. Kleihaus, and J. Kunz, Phys. Rev. D **65**, 024027 (2001).
[24] B. Kleihaus and J. Kunz, Phys. Rev. Lett. **85**, 2430 (2000).
[25] B. Kleihaus and J. Kunz, Phys. Lett. B **494**, 130 (2000).
[26] J. Van der Bij and E. Radu, Int. J. Mod. Phys. A **17**, 1477 (2002).
[27] V. Paturyan and D. Tchrakian, J. Math. Phys. (N.Y.) **45**, 302 (2004).
[28] V. Paturyan, E. Radu, and D. Tchrakian, Phys. Lett. B **609**, 360 (2005).
[29] B. Kleihaus, J. Kunz, and F. Navarro-Lerida, Phys. Lett. B **599**, 294 (2004).
[30] B. Kleihaus, J. Kunz, and Y. Shnir, Phys. Rev. D **71**, 024013 (2005).
[31] B. Kleihaus, J. Kunz, and U. Neemann, Phys. Lett. B **623**, 171 (2005).
[32] O. Hauser, R. Ibadov, B. Kleihaus, and J. Kunz, Phys. Rev. D **89**, 064010 (2014).
[33] R. Bartnik and J. McKinnon, Phys. Rev. Lett. **61**, 141 (1988).
[34] R. R. Caldwell, Phys. Lett. B **545**, 23 (2002).
[35] S. M. Carroll, M. Hoffman, and M. Trodden, Phys. Rev. D **68**, 023509 (2003).
[36] G. Gibbons, arXiv:hep-th/0302199.
[37] S. Hannestad, Int. J. Mod. Phys. A **21**, 1938 (2006).

[38] K. A. Bronnikov and J. C. Fabris, Phys. Rev. Lett. **96**, 251101 (2006).
[39] S. Chen, M. Wang, and J. Jing, Classical Quantum Gravity **33**, 195002 (2016).
[40] B. Kleihaus, J. Kunz, and E. Radu, Phys. Lett. B **797**, 134892 (2019).
[41] V. Dzhunushaliev, V. Folomeev, R. Myrzakulov, and D. Singleton, J. High Energy Phys. 07 (2008) 094.
[42] H. G. Ellis, J. Math. Phys. (N.Y.) **14**, 104 (1973).
[43] H. G. Ellis, Gen. Relativ. Gravit. **10**, 105 (1979).
[44] K. A. Bronnikov, Acta. Phys. Pol. **B4**, 251 (1973).
[45] M. Visser, *Lorentzian Wormholes: From Einstein to Hawking* (AIP, Woodbury, USA, 1995).
[46] P. Kanti, B. Kleihaus, and J. Kunz, Phys. Rev. Lett. **107**, 271101 (2011).
[47] P. Kanti, B. Kleihaus, and J. Kunz, Phys. Rev. D **85**, 044007 (2012).
[48] G. Antoniou, A. Bakopoulos, P. Kanti, B. Kleihaus, and J. Kunz, Phys. Rev. D **101**, 024033 (2020).
[49] J. Gonzalez, F. Guzman, and O. Sarbach, Classical Quantum Gravity **26**, 015010 (2009).
[50] J. Gonzalez, F. Guzman, and O. Sarbach, Classical Quantum Gravity **26**, 015011 (2009).
[51] T. Torii and H.-a. Shinkai, Phys. Rev. D **88**, 064027 (2013).
[52] P. Kashargin and S. Sushkov, Gravitation Cosmol. **14**, 80 (2008).
[53] P. Kashargin and S. Sushkov, Phys. Rev. D **78**, 064071 (2008).
[54] B. Kleihaus and J. Kunz, Phys. Rev. D **90**, 121503 (2014).
[55] X. Y. Chew, B. Kleihaus, and J. Kunz, Phys. Rev. D **94**, 104031 (2016).
[56] V. Dzhunushaliev, V. Folomeev, B. Kleihaus, J. Kunz, and E. Radu, Phys. Rev. D **88**, 124028 (2013).
[57] X. Y. Chew, B. Kleihaus, and J. Kunz, Phys. Rev. D **97**, 064026 (2018).
[58] P. G. Nedkova, V. K. Tinchev, and S. S. Yazadjiev, Phys. Rev. D **88**, 124019 (2013).
[59] G. Gyulchev, P. Nedkova, V. Tinchev, and S. Yazadjiev, Eur. Phys. J. C **78**, 544 (2018).
[60] M. Amir, A. Banerjee, and S. D. Maharaj, Ann. Phys. (Amsterdam) **400**, 198 (2019).
[61] F. Abe, Astrophys. J. **725**, 787 (2010).
[62] Y. Toki, T. Kitamura, H. Asada, and F. Abe, Astrophys. J. **740**, 121 (2011).
[63] R. Takahashi and H. Asada, Astrophys. J. Lett. **768**, L16 (2013).
[64] J. G. Cramer, R. L. Forward, M. S. Morris, M. Visser, G. Benford, and G. A. Landis, Phys. Rev. D **51**, 3117 (1995).
[65] V. Perlick, Phys. Rev. D **69**, 064017 (2004).
[66] N. Tsukamoto, T. Harada, and K. Yajima, Phys. Rev. D **86**, 104062 (2012).
[67] C. Bambi, Phys. Rev. D **87**, 107501 (2013).
[68] M. Zhou, A. Cardenas-Avendano, C. Bambi, B. Kleihaus, and J. Kunz, Phys. Rev. D **94**, 024036 (2016).
[69] J. L. Blázquez-Salcedo, X. Y. Chew, and J. Kunz, Phys. Rev. D **98**, 044035 (2018).
[70] P. Hajicek, Proc. R. Soc. A **386**, 223 (1983).
[71] P. Hajicek, J. Phys. A **16**, 1191 (1983).
[72] F. Degen, Gen. Relativ. Gravit. **19**, 739 (1987).
[73] V. Dzhunushaliev, V. Folomeev, C. Hoffmann, B. Kleihaus, and J. Kunz, Phys. Rev. D **90**, 124038 (2014).
[74] C. Hoffmann, T. Ioannidou, S. Kahlen, B. Kleihaus, and J. Kunz, Phys. Rev. D **95**, 084010 (2017).
[75] A. Corichi, U. Nucamendi, and D. Sudarsky, Phys. Rev. D **62**, 044046 (2000).
[76] A. Ashtekar, A. Corichi, and D. Sudarsky, Classical Quantum Gravity **18**, 919 (2001).
[77] U. Ascher, J. Christiansen, and R. D. Russell, Math. Comput. **33**, 659 (1979).
[78] B. Kleihaus, J. Kunz, and P. Kanti, Phys. Rev. D **102**, 024070 (2020).
[79] X. Y. Chew and K.-G. Lim (to be published).
[80] V. Dzhunushaliev, V. Folomeev, B. Kleihaus, and J. Kunz, Phys. Rev. D **87**, 104036 (2013).
[81] V. Dzhunushaliev, V. Folomeev, B. Kleihaus, and J. Kunz, Phys. Rev. D **89**, 084018 (2014).
[82] A. Aringazin, V. Dzhunushaliev, V. Folomeev, B. Kleihaus, and J. Kunz, J. Cosmol. Astropart. Phys. 04 (2015) 005.
[83] B. R. Greene, S. D. Mathur, and C. M. O'neill, Phys. Rev. D **47**, 2242 (1993).
[84] E. Winstanley and N. E. Mavromatos, Phys. Lett. B **352**, 242 (1995).
[85] N. E. Mavromatos and E. Winstanley, Phys. Rev. D **53**, 3190 (1996).